COMSOL
CONFERENCE
2023 MUNICH

Analysis and Comparison of Modeling Approaches for Heat Pipes

L. Fromme, N. Peick, L. M. Sommer
Faculty of Engineering and Mathematics, Hochschule Bielefeld – University of Applied Sciences and Arts (HSBI), Bielefeld, Germany

Abstract
Two heat pipe cycle process models are built in the simulation software COMSOL Multiphysics based on the modeling approaches available in the COMSOL Application Gallery (ID 43841 [1] and 90311 [2]). Both approaches are projected onto the geometry of a tubular heat pipe for which relevant thermodynamic parameters (saturation temperature and pressure, heat transfer rate) are measured experimentally. The simulation results for temperature, pressure and flow velocity are analyzed and evaluated.

Keywords: heat pipe, evaporation, condensation, latent heat, two-phase fluid flow, capillary circulation

Introduction
A novel injection molding tool temperature control system based on heat pipes is being researched at the Bielefeld University of Applied Sciences and Arts (HSBI). This temperature control technology offers great potential for improving product quality and saving energy in the production process [3-6]. Heat pipes have a hermetically sealed and evacuated working chamber containing a working fluid (distilled water), which serves as a highly efficient heat transfer medium (latent heat) in a thermodynamic cycle (evaporation and condensation). The latent heat transfer occurs through the vapor flow inside the heat pipe working chamber, which can be described by the physical state variables of flow velocity, pressure, temperature, and density. These physical state variables are difficult to measure, so it is of interest to approximate the basic functioning of the thermodynamic heat pipe cycle process through numerical simulation and determine the physical state variables approximately.

Theory
Heat pipes are tubes that are evacuated and then filled with a working fluid and are permanently sealed. Its inside walls are lined with a capillary structure (also known as wick). Such pipes achieve a very high thermal energy conductance by means of two-phase fluid flow with capillary circulation. Figure 1 shows the thermodynamic heat pipe cycle, which is divided into four continuous process steps: evaporation, vapor flow, condensation, and liquid flow. These process steps can be assigned to the three functional sections of a heat pipe: heat source (evaporator), adiabatic zone, and heat sink (condenser).

Heat added to the evaporator causes a phase change of the working fluid from liquid to vapor phase at the surface of the capillary structure. The local vapor pressure in this section increases and the vapor flows toward the condenser. The latent heat is transported from the heat source to the heat sink by means of the vapor flow. At the condenser section, condensation of the vapor occurs at the surface of the capillary structure, releasing the latent heat. Subsequently, the liquid is drawn back to the evaporator area by capillary action, where it is vaporized again to continue the cycle [7,8].

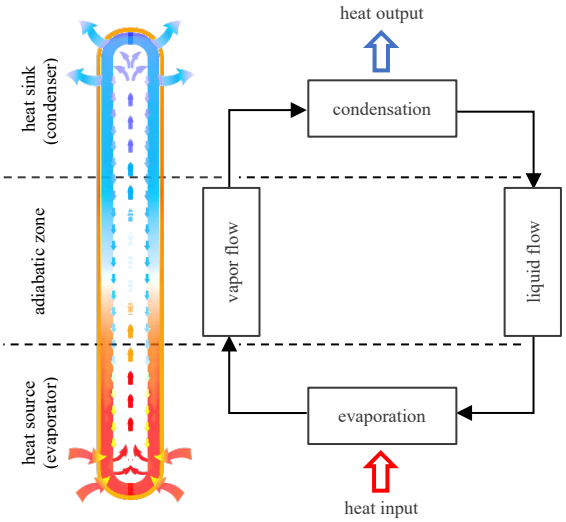

Figure 1. Thermodynamic heat pipe cycle process

Inside a heat pipe, the temperature gradient along the length is very small. Evaporation at the hot end requires a heat source wall temperature level that is slightly above the saturation temperature of the working fluid whereas condensation at the cold end requires a heat sink wall temperature slightly below the saturation temperature. The most efficient and effective heat exchange between the heat source and the heat sink requires thermal separation, which is represented by the adiabatic transport zone, so that ideally no heat exchange with the environment can occur in this section. Altogether, heat can be transported over long distances with insignificant temperature drop [5].

Depending on the application, the described continuous thermodynamic cycle can be used for heat removal as well as for heat supply [3].

Experimental Set-Up and Numerical Models

Two heat pipe cycle process models are built in the simulation software COMSOL Multiphysics based on the two different modeling approaches available in COMSOL`s Application Gallery (Application ID 43841 and 90311), which are projected onto the heat pipe geometry to be analyzed, as shown in Figure 2. Respectively, a stationary study is used in the numerical models to analyze heat pipe running at its design point. Due to the axisymmetric geometry of the heat pipe, the modeling is done in two dimensions (see Fig. 2).

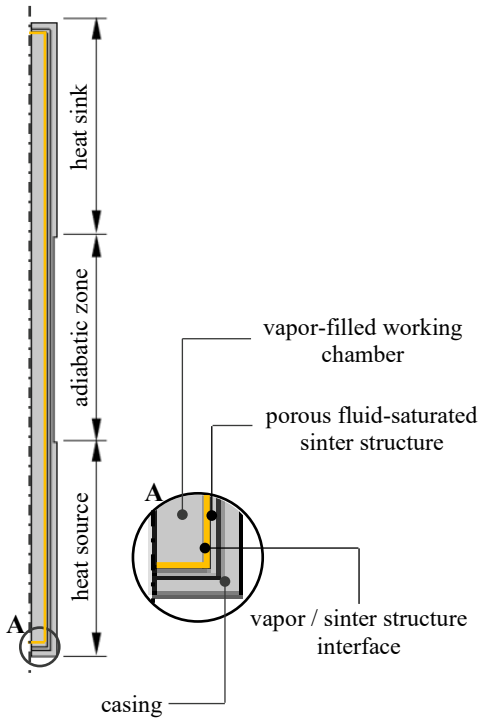

Figure 2. Axisymmetric heat pipe geometry.

The heat pipe geometry consists of the vapor-filled working chamber, which is enclosed by a porous fluid-saturated sinter structure and the heat pipe casing. It is divided into three functional sections: heat source, adiabatic transport zone, and heat sink. The three functional zones have an identical length of 66 mm each. The inner diameter of the vapor chamber is 10 mm.

As working fluid distilled water is used, which exists in both liquid and vapor state in the cycle process. Therefore, it is necessary to assign appropriate material properties for each state. The porous sinter structure and the heat pipe casing are made of a copper alloy. The material definitions in both model approaches differ in a few points. The model approach 1 (ID 43841) does not consider temperature and pressure dependence of the physical material properties. Only the density of the working fluid in the vapor state is approximated using the ideal gas law. On the other hand, in model approach 2 (ID 90311) the temperature- and pressure-dependent material data is taken from COMSOL's new built-in thermodynamics database, which is available in the Liquid & Gas Properties module.

As explained above, the continuous heat pipe cycle process consists of four consecutive process steps. For a realistic representation these steps need to be modeled in the numerical simulation somehow. The modeling strategies for the process steps of the analyzed model approaches are described below, along with their differences.

- **heat input (evaporator)**

The heat transfer rate to be transferred by the heat pipe is defined as a constant heat flux over the outer heat source surface as a boundary condition, with a magnitude of $\dot{Q}_{\mathrm{tot}} = 170$ W at the operating point of interest.

- **vapor flow**

The vapor flow in the heat pipe working chamber, which significantly describes the transport of latent heat between the heat source and the heat sink, is modeled as compressible laminar flow in both model approaches. The flow is induced by a pressure difference between the heat source and the heat sink. Therefore, the boundary condition of the vapor flow domain is set to the temperature-dependent saturation pressure, which implies that the liquid and vapor phase are assumed to be in equilibrium at the interface between the vapor chamber and the porous fluid-saturated sinter structure (see orange-marked area in Figure 2). This saturation pressure differs between the two model approaches. Model approach 1 approximates the saturation pressure using the Clausius-Clapeyron equation, as shown in equation (1).

$$p_{\mathrm{sat},1} = p_{\mathrm{ref}} \cdot e^{\frac{h_{\mathrm{vap}} \cdot M_{\mathrm{n}}}{R} \cdot \left(\frac{1}{T_{\mathrm{ref}}} - \frac{1}{T}\right)} \qquad (1)$$

The Clausius-Clapeyron equation calculates the saturation pressure p_{sat} as a function of temperature T, assuming a known reference point on the saturation pressure curve (pressure p_{ref} and temperature T_{ref}), as well as the vaporization enthalpy h_{vap}, molar mass M_{n} and the universal gas constant R. The vaporization enthalpy is simplified as a constant. In contrast, model approach 2 uses a function from the thermodynamics database for the saturation pressure, as shown in equation (2).

$$p_{\mathrm{sat},2} = p_{H_2O,\mathrm{sat}}(T) \qquad (2)$$

The evaporation and condensation processes are not explicitly modeled in both model approaches. The supplied or dissipated heat transfer rate is calculated based on the vapor flow, which enters or exits the vapor chamber through the previously described interface. For this purpose, the interface area is

defined as a boundary heat source (for heat input or heat dissipation). The latent heat of vaporization $\dot{q}_{\mathrm{vap}}$ is calculated using the following equation (3).

$$\dot{q}_{\mathrm{vap}} = \dot{m} \cdot h_{\mathrm{vap}} \qquad (3)$$

Here, $\dot{m}$ denotes the vapor mass flow rate and h_{vap} represents the vaporization enthalpy, which is assumed to be constant in model approach 1. In model approach 2, on the other hand, the temperature-dependent vaporization enthalpy from the thermodynamics database is used.

Since the saturation pressure increases exponentially with increasing temperature, the vapor flow occurs from high-temperature regions to low-temperature regions. Thus, heat is dissipated at the heat source (high temperature and high pressure) and supplied at the heat sink side (low temperature and low pressure).

- **heat output (condenser)**

The heat energy supplied at the heat source, which is transported to the heat sink through the phase change of the working fluid as well as solid heat conduction, must be dissipated to the surroundings through the surface of the heat sink. For this purpose, a convective heat flux boundary condition is defined on the outer surface of the heat sink, as shown in equation (4).

$$\dot{Q}_{\mathrm{conv}} = h_{\mathrm{conv}} \cdot (T_{\mathrm{ext}} - T) \cdot A_{\mathrm{ws}} \qquad (4)$$

The convective heat transfer rate $\dot{Q}_{\mathrm{conv}}$ is calculated as the product of the heat transfer coefficient h_{conv}, the temperature difference between the ambient temperature T_{ext} and the heat sink surface temperature T, and the heat sink surface area A_{ws}. No heat exchange occurs over the surface of the adiabatic transport zone, as it is idealized as thermally isolated in the simulation.

- **liquid flow**

The backflow of the condensed working fluid along the inner walls of the pipe from the heat sink through the adiabatic transport zone back to the heat source is not explicitly modeled in model approach 1. Instead, a time-constant fluid-saturated porous sinter structure is assumed. In model approach 2, however, the flow of the condensed fluid through the fluid-saturated porous sinter structure is additionally modeled using the Brinkman equations. These equations describe the liquid flow through a porous material. Since there must be a mass flow equilibrium between the evaporated and condensed fluid quantities in the steady state of the thermodynamic heat pipe cycle process, the mass flows of the working fluid in the liquid and vapor phases are equated. Since both mass flows refer to the interface between the vapor and liquid flow, it is sufficient to consider the ratio of the product of the flow velocity $\vec{u}$ and the density ρ, as shown in equation (5).

$$\vec{u}_V \cdot \rho_V = \vec{u}_L \cdot \rho_L \qquad (5)$$

The index L refers to the working fluid in the liquid phase, while the index V refers to the vapor phase.

The coupling of heat transfer and laminar flow, as well as the additional liquid backflow in the case of model approach 2, is achieved through the multiphysics coupling "Nonisothermal Flow". This coupling is necessary because flow properties, such as density, depend on the temperature.

Simulation Results

In both modeling approaches the wick structure is assumed to be saturated with liquid water, corresponding to the heat pipe running at its design point. For comparison of the simulation results the distributions of temperature, pressure and flow velocity are analyzed.

Figure 3 illustrates the temperature distribution in the cross-section of the axisymmetric heat pipe geometry and compares the results of the two model approaches.

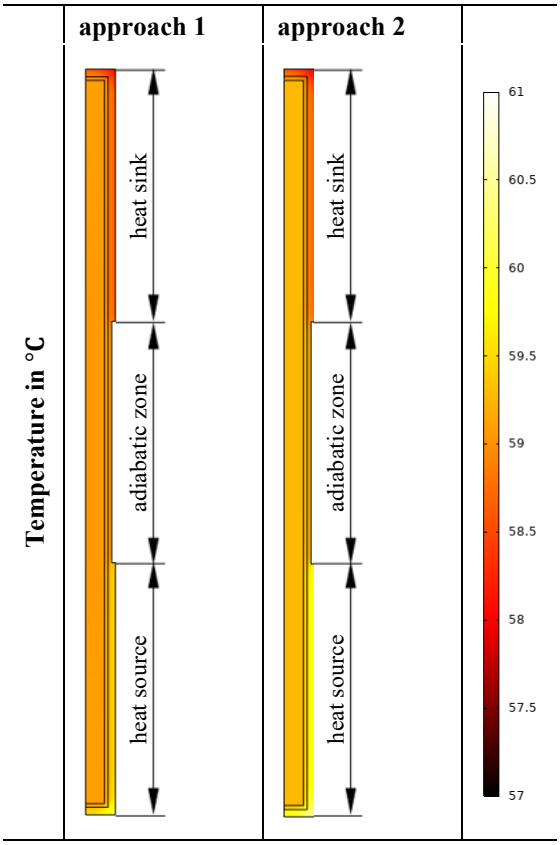

Figure 3. Temperature distributions for both modeling approaches.

As expected, both model approaches exhibit the highest temperatures at the outer surface of the heat source. In this region, it is evident that the maximum temperature of model approach 2 is higher than that

of model approach 1. The lowest temperature is observed at the outer surface of the heat sink, where both model approaches show nearly identical temperature values due to the identical boundary conditions for convective heat dissipation. Furthermore, there is a slight difference in the temperature distributions in the casing, in the wick structure as well as in the vapor chamber. Of course, the vapor temperature appears nearly isothermal throughout in both model approaches, but it is slightly higher in model approach 2. The average vapor temperature in model approach 1 is approximately 59,1 °C, while it is about 59,3 °C in model approach 2.

Figure 4 illustrates the resulting pressure profiles in the vapor-filled heat pipe working space.

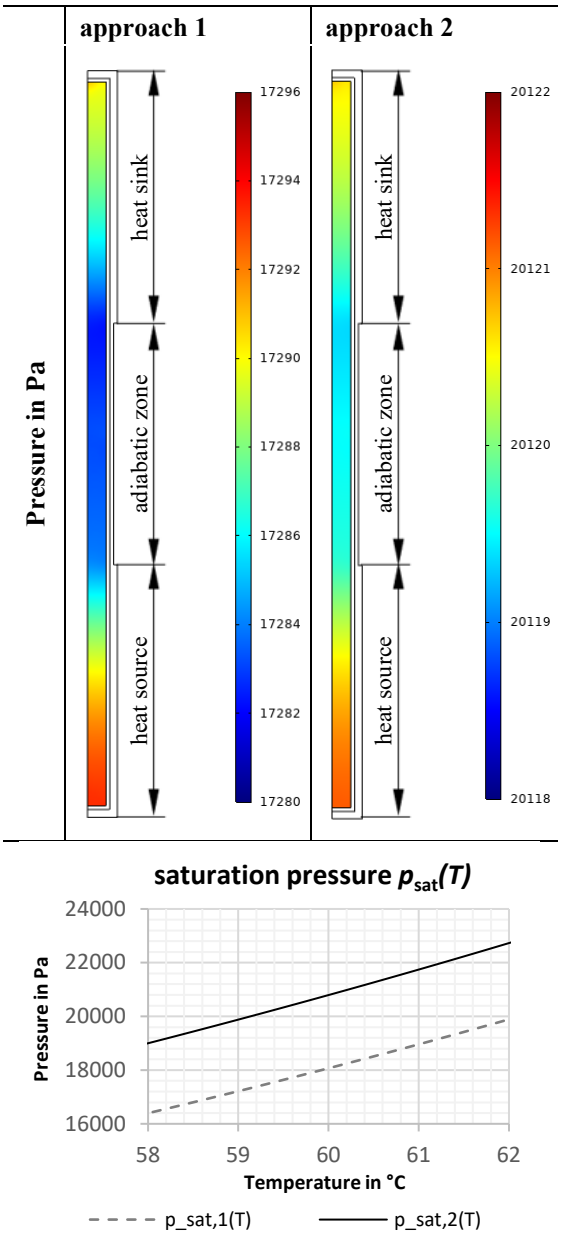

Figure 4. Pressure distributions in the vapor chamber and the saturation pressure curves for both modeling approaches, also compare equations (1) and (2).

The determination of pressure at the interface between the water-saturated porous sinter structure and the vapor-filled heat pipe working space is based on the temperatures prevailing at the interface, as described in the model formulation. The temperature-pressure coupling is achieved through the saturation pressure curve of the working fluid. It is evident that the model approaches differ significantly in terms of pressure levels. The reasons for this lie in the different approximations of the temperature-dependent saturation pressure curves and the minimal temperature differences at the interface itself. The diagram in Figure 4 shows a section of the two saturation pressure curves in the temperature range relevant for the simulations. In this temperature range, the two curves have a pressure difference of approximately 2700 Pa. Furthermore, both model approaches exhibit a pressure difference between the heat source and heat sink. But the pressure difference in model approach 1 is significantly more pronounced in magnitude.

Apparently, these significantly different pressure differences between the heat source and heat sink also result in different vapor flow velocities in the two model approaches, as shown in Figure 5.

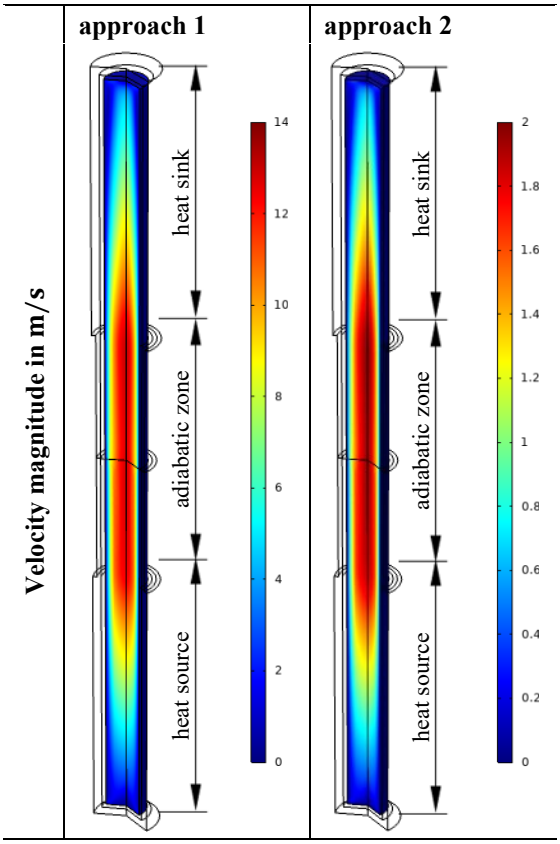

Figure 5. Flow velocity profiles in the vapor chamber for both modeling approaches.

It can be observed that the maximum flow velocity of approach 1 is almost seven times greater than that of approach 2. This is because the density in the approach depicted on the left is proportionally lower, while the velocity is higher (approach 1:

$\rho = 0{,}11274\ \frac{\text{kg}}{\text{m}^3}$, approach 2: $\rho = 0{,}79158\ \frac{\text{kg}}{\text{m}^3}$). This relationship arises from both models transporting the same mass flow rate of vapor.

When considering the energy balance of the latent heat transfer rate $\dot{Q}_{\text{vap}}$ in the circular cross-section in the middle of the heat pipe working space, it becomes apparent that almost the entire heat transfer between the heat source and heat sink occurs through latent heat transfer ($\dot{Q}_{\text{tot}} = 170\ \text{W}$ and $\dot{Q}_{\text{vap}} = 169{,}68\ \text{W}$). Thus, heat conduction in the heat pipe casing and porous sinter structure plays a subordinate role in the overall energy balance. The two model approaches have identical values for the transferred latent heat transfer rate.

Experimental Results and Simulation Validation

The previously compared simulation results of the two model approaches are now being evaluated using experimentally determined measurement data and steam pressure table values.

Significant differences have been observed, especially in terms of pressure level and flow velocity, so the saturation pressure curve, density of the working fluid in the vapor state, and the enthalpy of vaporization are considered. Additionally, the heat transfer capacity of the heat pipe at the simulation operating point is compared to the experimental measurement data.

- **saturation pressure**

In both modeling approaches the saturation temperature in the considered operating point is approximately 59 °C. In the experimental set-up, this saturation temperature corresponds to a pressure range between 19000 Pa and 21000 Pa. The pressure range is due to the discontinuous boiling process and the associated pressure fluctuations in the heat pipe working space. The measured pressure data also reflect the expected pressure at the given saturation temperature and can be obtained from steam pressure tables of the working fluid. Comparing these pressure values with the saturation pressure curves used in the simulation, as shown in Figure 4, it turns out that the approximation using the Clausius-Clapeyron equation yields pressure values of approximately 17200 Pa, while the saturation pressure function implemented in COMSOL's thermodynamics database yields pressure values of approximately 19900 Pa. Thus, the saturation pressure values are more accurately represented in model approach 2.

- **working fluid density in the vapor phase and enthalpy of vaporization**

The enthalpy of vaporization, which is assumed to be constant in model approach 1 compared to the temperature-dependent one used in model approach 2, differs only moderately in the considered operating point. However, a significant difference in densities can be observed. This is due to the different temperatures and pressures appearing in the heat pipe working space. Using the ideal gas law to approximate the working fluid density in the vapor phase has a much greater influence on the density difference. Again, the simulation results of model approach 2 are more precise due to the thermodynamics data implemented in COMSOL.

- **heat transfer capacity**

Figure 6 shows the experimentally recorded characteristic field of heat pipe (z-axis heat transfer capacity in W) as a function of the heat source temperature (y-axis T_{wq} in °C) and its temperature difference to the heat sink temperature (x-axis $\Delta T = T_{\text{wq}} - T_{\text{ws}}$ in °C).

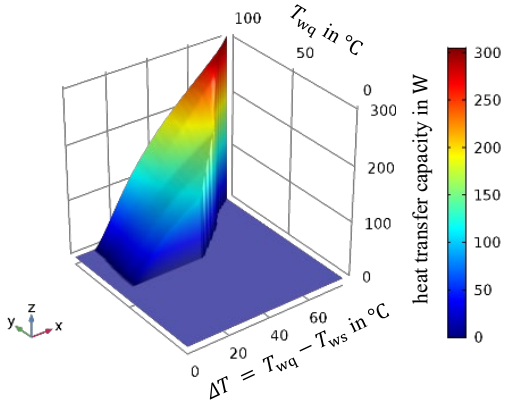

Figure 6. The characteristic map of the heat pipe shows the heat transfer capacity as a function of local temperatures.

Apparently, the heat transfer capacity of the heat pipe to be transferred, which is 170 W in the case under consideration, can occur at various temperature combinations of the heat source and heat sink.

The modeling of the heat pipe cycle process only considers the geometric dimensions. However, the heat transfer capacity depends on a variety of other parameters, such as the internal pressure of the working space at room temperature, the fluid fill level, and the temperature levels at the heat source and heat sink. Furthermore, the evaporation and condensation mechanisms, as well as the performance limits, are not considered in detail. However, these factors can have a significant influence on the heat transfer capacity of the heat pipe.

It should be noted that the fundamental functionality of the thermodynamic heat pipe cycle process could be represented by the simulation. Model approach 2 was able to provide more accurate results, mainly due to the temperature- and pressure-dependent

properties of density, enthalpy of vaporization, and the saturation pressure function implemented in COMSOL's thermodynamics database. However, a complete simulation-driven design of the heat transfer capacity of the heat pipe is not possible due to the strong simplification of the evaporation and condensation processes and the lack of initial conditions (pressure and fluid fill level in the heat pipe working space).

Therefore, model approach 2 must be adjusted to gain insights into the real flow velocity in the heat pipe working space. For this purpose, the experimentally determined measurement data of the heat transfer capacity and saturation temperature is incorporated into the extended simulation model using characteristic fields. The operating point to be considered is chosen in such a way that the magnitude of the heat flux to be transferred corresponds to that from the previous simulation runs. The simulation results are presented below.

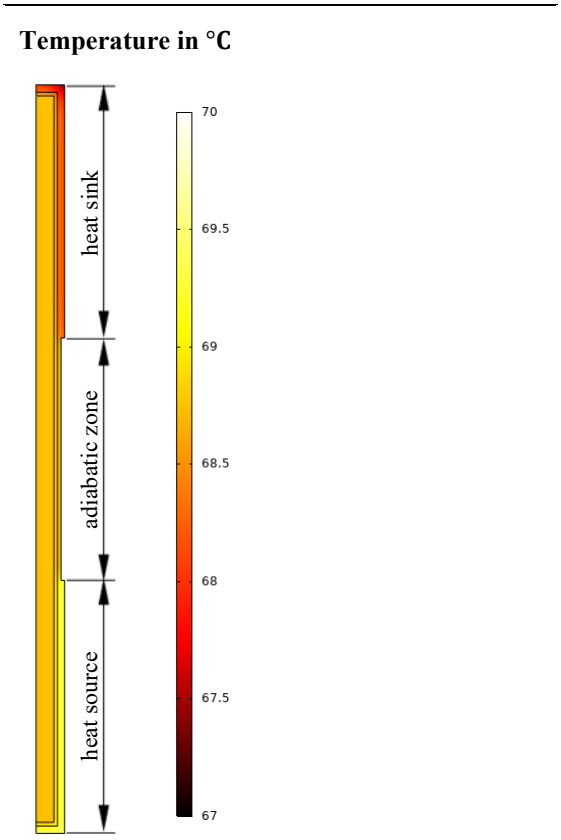

Figure 7. Temperature distribution in the heat pipe (map).

The resulting temperature distribution, which is shown in Figure 7, has in principle a similar shape as in the case described above. However, due to the experimentally determined saturation temperature specified on the outer surface of the heat source, the temperature level is higher compared to the previous simulation results.

It turns out that the saturation temperature in the considered operating point in this case is approximately 68,8 °C. The effects of the higher temperature level on pressure and the dependent flow velocity are shown in Figure 8. Due to the coupling of temperature and pressure through the saturation pressure function of the working fluid, the higher temperature is also associated with an increase in pressure in the vapor chamber. However, the pressure difference between the heat source and heat sink is of a similar magnitude as in the simulation results of model approach 2. As a result, the flow velocity differs only slightly from model approach 2 due to the different densities of the working fluid in the vapor state and the different enthalpies of vaporization.

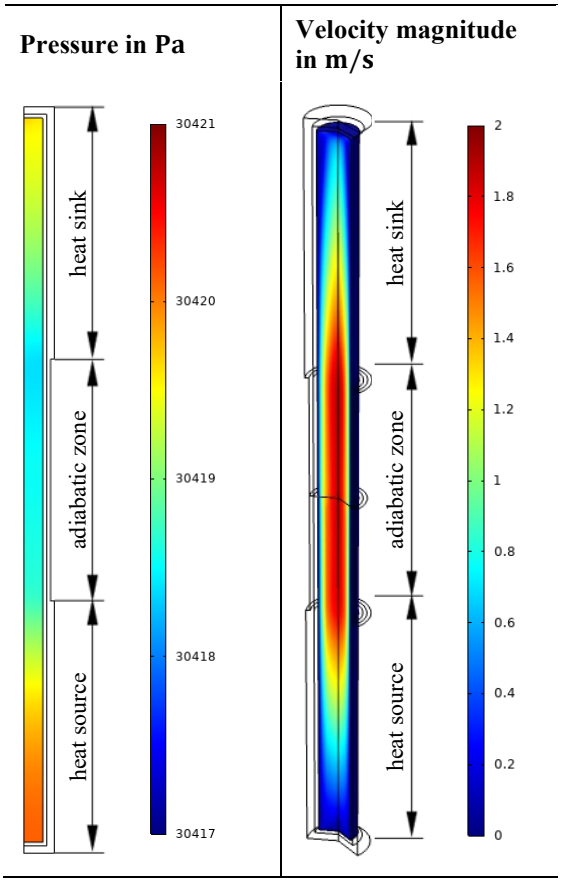

Figure 8. Pressure distribution and flow velocity profile in the heat pipe working space (map).

Conclusions

Based on two different modeling approaches available in the COMSOL Application Gallery, the fundamental functionality of the thermodynamic heat pipe cycle process could be represented. It should be noted that a high accuracy of temperature- and pressure-dependent fluid properties (saturation temperature and pressure, density, enthalpy of vaporization) is necessary for modeling vapor flow inside the heat pipe working chamber. Approximating the working fluid density in the vapor phase using the ideal gas law, as well as approximating the saturation pressure function using

the Clausius-Clapeyron equation, leads to significant losses in result quality.

Comparing the simulation results with the experimentally measured data allows calibration of the simulation model at the operating point under consideration and thus the approximate determination of the physical state variables inside the heat pipe working chamber. A more detailed modeling of the heat pipe cycle process requires an extension of the model to include the evaporation and condensation processes, as well as consideration of the initial conditions (temperature, pressure and fluid fractions in the heat pipe working chamber).

References

[1] COMSOL, *Flat Heat Pipe*, Application Gallery, Application ID: 43841, as of September 2021, https://www.comsol.com/model/flat-heat-pipe-43841

[2] COMSOL, *Heat Pipe with Accurate Liquid and Gas Properties*, Application Gallery, Application ID: 90311, as of September 2022, https://www.comsol.com/model/heat-pipe-with-accurate-liquid-and-gas-properties-90311

[3] C. Jaroschek, S. Kartelmeyer, V. Hüttemann, *"No Cool" Molds, Properly Simulated*, Kunststoffe international, pp. 30-33, 08 2017.

[4] S. Kartelmeyer, C. Jaroschek, E. Moritzer, *Temperieren ohne Wasser - Einsatz von Heatpipes in Spritzgießwerkzeugen*, VDWF im Dialog, pp. 20-25, 04 2018.

[5] S. Kartelmeyer, C. Jaroschek, L. Fromme, V. Hüttemann, E. Moritzer, *Thermal Simulation of a Heat Pipe Tempered Injection Mould Tool*, Comsol Conference, Lausanne, 2018.

[6] S. Kartelmeyer, V. Hüttemann, E. Moritzer, C. Jaroschek, *Simulation and Testing of a Heat Pipe Tempered Injection-Mold vs. Conventional Water-Based Cooling*, Conference Proceedings SPE Antec, Detroit, Detroit, 2019.

[7] A. C. Griesinger, *Wärmemanagement in der Elektronik: Theorie und Praxis*, Berlin, Heidelberg: Springer, 2019.

[8] B. Zohuri, Hg., *Functionality, Advancements and Industrial Applications of Heat Pipes*, London: Academic Press, 2020.